

This is the author's peer reviewed, accepted manuscript. However, the online version of record will be different from this version once it has been copyedited and typeset.
PLEASE CITE THIS ARTICLE AS DOI: 10.1063/5.0061997

Microfluidic model of monocyte extravasation reveals the role of hemodynamics and subendothelial matrix mechanics in regulating endothelial integrity

Sandra Pérez-Rodríguez^{1,2}, Stephanie A Huang³, Carlos Borau^{1,2}, José Manuel García-Aznar^{1,2}, William J Polacheck^{3,4,5}*

¹Multiscale in Mechanical and Biological Engineering, Department of Mechanical Engineering, University of Zaragoza, 50018 Zaragoza, Spain

²Aragon Institute of Engineering Research, University of Zaragoza, 50018 Zaragoza, Spain

³Joint Department of Biomedical Engineering, University of North Carolina at Chapel Hill and North Carolina State University, Chapel Hill, North Carolina, 27599, USA.

⁴McAllister Heart Institute, University of North Carolina at Chapel Hill School of Medicine, Chapel Hill, North Carolina, 27599, USA.

⁵Department of Cell Biology and Physiology, University of North Carolina at Chapel Hill School of Medicine, Chapel Hill, North Carolina, 27599, USA.

* Correspondence: polacheck@unc.edu ; Tel.: +1 919-966-3880

ABSTRACT

Extravasation of circulating cells is an essential process that governs tissue inflammation and the body's response to pathogenic infection. To initiate anti-inflammatory and phagocytic functions within tissues, immune cells must cross the vascular endothelial barrier from the vessel lumen to the subluminal extracellular matrix. In this work, we present a microfluidic approach that enables the recreation of a three-dimensional, perfused endothelial vessel formed by human endothelial cells embedded within in a collagen-rich matrix. Monocytes are introduced into the vessel perfusate, and we investigate the role of luminal flow and collagen concentration on extravasation. In vessels conditioned with flow, increased monocyte adhesion to the vascular wall was observed, though fewer monocytes extravasated to the collagen hydrogel. Our results suggest the lower rates of extravasation are due to the increased vessel integrity and reduced permeability of the endothelial monolayer. We further demonstrate that vascular permeability is a function of collagen hydrogel mass concentration, with increased collagen concentrations leading to elevated vascular permeability and increased extravasation. Collectively, our results demonstrate that extravasation of monocytes is highly regulated by the structural integrity of the endothelial monolayer. The microfluidic approach developed here allows for the dissection of the relative contributions of these cues to further understand the key governing processes that regulate circulating cell extravasation and inflammation.

SIGNIFICANCE

A 3D microfluidic model of the vascular endothelium perfused with circulating monocytes is developed to determine the role of hemodynamics and matrix mechanics in governing monocyte adhesion, transmigration, and infiltration of tissues.

INTRODUCTION

Extravasation is the process by which cells and proteins traverse the endothelial barrier from the intravascular cannula into surrounding tissue [1]. During an inflammatory injury or bacterial infection, immune cells extravasate in response to mechanical and chemical stimuli secreted by damaged tissues [2]. In this work, we focus specifically on monocyte extravasation due to its essential role in homeostasis and the development of innate and adaptive immune responses to pathogens [3]. While a number of cellular and molecular regulators of extravasation have been identified using conventional *in vitro* approaches [4], interpreting these results in the context of the native microenvironment is challenging due to limitations to *in vitro* culture systems, including the lack of physiologic tissue architecture and mechanics. Here, we seek to address these shortcomings through the implementation of a microfluidic multi-cell culture system that more closely mimics the native architecture and mechanics of the microvasculature.

Monocyte extravasation is initiated through the coordination of receptor-mediated interactions between the apical surface of vascular endothelial cells and monocytes. First, immune cells from damaged tissue secrete inflammatory cytokines that induce the expression of adhesion molecules in endothelial cells. E- and P-selectin, intercellular adhesion molecule 1 (ICAM-1) and vascular cell adhesion molecule 1 (VCAM-1) have been specifically implicated in monocyte-endothelial interactions [5]. ICAM-1 and VCAM-1 contribute to monocyte adhesion [6], and VCAM-1 reduces rolling speed and enhances firm arrest [7]. Additionally, monocytes have basal expression of P-selectin Glycoprotein Ligand 1 (PSGL-1), which interacts with endothelial selectins, allowing for the attachment and rolling

of monocytes [8]. Once monocytes attach to the endothelial wall, an increase in endothelial RhoA GTPase-mediated actomyosin contractility in endothelial cells induces intercellular junction disassembly and the formation of transient gaps in the monolayer [9]. Finally, monocytes generate protrusions to probe the endothelial surface and cross the endothelial barrier [10], [11].

Hemodynamics play a critical role in extravasation through modulating protein expression and signaling in endothelial cells. Fluid shear stress between 2 and 10 dynes/cm² upregulates the expression of E-selectin, P-selectin, ICAM-1 and VCAM-1 on endothelial cells, leading to an increase in monocyte arrest at the endothelial wall [12]–[14]. Conversely, endothelial cells exposed to physiological shear stress, in a range between 3 and 5 dynes/cm², suppress RhoA signaling and upregulate Rac1 signaling, resulting in adherens junction assembly and cytoskeletal alignment [15]–[17]. Therefore, hemodynamic shear stress imparts competing signals on the extravasation process by increasing monocyte arrest to the endothelium, but strengthening the vascular barrier. Further dissection of these mechanisms necessitates the development of a platform in which vascular endothelial cells and monocytes can be cultured in a hemodynamic environment and observed in real time.

Signals from the basal surface of the endothelium, including the perivascular extracellular matrix, have also been shown to play a role in extravasation. Vascular endothelial cells are highly sensitive to the stiffness of the underlying matrix [18], and pathologically increased matrix stiffness drives increases in vascular permeability [19]. Substrate mechanics also play a role in monocyte adhesion. For example, Mackay and Hammer observed increased monocyte attachment to hydrogels coated with E-selection as a function of stiffness, but they found no stiffness-dependence for gels coated with P-selectin [20], highlighting the complex interplay between biochemical and biophysical cues in extravasation. Moreover, stiffer substrates are required to properly recruit and stabilize ICAM-1 on endothelial cells [21]. Collectively, these studies demonstrate that investigation of the key factors and molecular mediators that govern extravasation requires recapitulation of native perivascular matrix mechanics.

A variety of model systems have been developed to investigate the key molecular mechanisms that govern extravasation. Key chemokines secreted by monocytes, including interleukin-8 (IL-8) and monocyte chemoattractant protein-1 (MCP-1) which regulate firm monocyte adhesion and extravasation from the vascular endothelium, have been identified by molecular binding assays [22], [23]. Electrophoresis, microarrays, and polymerase chain reaction (PCR) techniques have allowed for the evaluation of monocyte and endothelial gene and protein expression that correlate with extravasation events in response to inflammatory factors. For example, lipopolysaccharides (LPS) induce E-selectin, VCAM-1 and ICAM-1 gene expression [24], whereas interferon gamma (INF- γ) and interleukin-4 (IL-4) upregulate MCP-1 mRNA and protein expression [25], [26]. In addition, electron microscopy has provided spatial resolution for key signaling pathways including IL-8, which, after being secreted by monocytes, is concentrated at the apical surface of endothelial cells prior to internalizations [27]. Furthermore, the combination of these data with animal models and computational simulations has elucidated possible models of paracellular and transcellular migration of leukocytes across endothelial barriers [28], [29], [30]. Despite enabling significant progress in identifying key governing pathways, these approaches have limitations, including a lack of physiological architecture and mechanics in *in vitro* systems

[31], and divergent mechanisms in mouse and human models [32], [33]. For example, the commonly used mice strain C57B1/6 exhibits cell-mediated immunity and Natural Killer (NK) cell activity that is significantly higher than other mice strains [34], and which is not representative of humans [35].

Microfluidic systems address some of these key limitations, particularly the need for more physiologic, three dimensional microenvironments *in vitro* [36], [37]. Recently, a number of microfluidic approaches have been developed for the study of extravasation [38]–[40], as recently reviewed Ma *et. al* [41]. However, the majority of these approaches are used to study cancer cell extravasation during metastasis, while the study of leukocytes and immune cell extravasation has received less attention. A few experimental approaches have been developed to study leukocyte extravasation in microfluidic devices, including endothelial cells cultured as a monolayer on a porous membrane [32], [42], [43], vascular networks embedded within collagen hydrogels [39], and endothelial monolayers attached to a rectangular PDMS channel [44]. Studies using these platforms have contributed to a fundamental and critical understanding of the mechanisms of extravasation, such as the relation between cancer cell extravasation and the expression of adenosine receptors [39] and late metastatic markers [44] or the inability of leukocytes to extravasate when treated with pertussis toxin [32]. However, there exist significant limitations in the physiological relevance of these approaches, including the lack of three-dimensional native architecture and/or physiologic substrate mechanics and hemodynamics.

Here, we present a microfluidic device and an approach that allows the formation of a continuous, lumenized, cylindrical monolayer of endothelial cells embedded within a collagen type-I matrix [45]. The diameter of this vessel varies between 150-250 μm , resembling physiological arterioles and venules [46], [47]. In vessels of this size, mechanotransduction of hemodynamic shear stresses facilitate interactions between immune and endothelial cells and immune cell extravasation [35], [48]. Using this platform, we demonstrate key aspects of physiological monocyte extravasation, including arrest to the apical vascular endothelial surface, crossing of the vascular endothelial barrier, and 3D migration through the hydrogel matrix. We further investigate the effect of hemodynamic shear stress and perivascular collagen concentration on extravasation, and the results of these studies demonstrate a critical role for biophysical stimuli in extravasation.

METHODS

Cell Culture

Human Umbilical Vein Endothelial Cells (HUVECs) were grown in EGM-2 medium supplemented with 2% of Fetal Bovine Serum (FBS), hydrocortisone, Vascular Endothelial Growth Factor (VEGF), R3 Insulin-Like Growth Factor 1 (R3 IGF-1), ascorbic acid, human Epidermal Growth Factor (hEGF), Gentamicin sulfate/Amphotericin (GA-1000) and heparin (medium EGM-2, Lonza, Basel, Switzerland). Cells were used from passage number 2 to 10, consistent with manufacturer recommendations to assure the viability and an adequate metabolism of cells.

THP-1 (ATCC® TIB202™, Manassas, VA, Unites States) is a commercial cell line of monocytes isolated from peripheral blood. THP-1 were grown in suspension in RPMI-1640 media supplemented with L-glutamine, 2% of FBS and Ampicillin/Streptomycin (RPMI-1640,

Gibco, Gaithersburg, MD, United States), and THP-1 were used from passage number 0 to 7.

Fabrication of Microfluidic Devices

Microfluidic devices (Fig. 1) were prepared following the protocol developed by Polacheck *et al.* [16], with minor modifications. Briefly, polydimethylsiloxane (PDMS) molds were generated by the mixture and degasification of the curing agent of Sylgard 184 silicone elastomer and the base in a 1:10 ratio, poured onto plastic molds replica molded from silicon master molds patterned by photolithography, and incubated at 60 °C for 24 h. Next, PDMS mold was separated from the plastic molds, and devices were individually cut and autoclaved. PDMS devices and glass coverslips (22 x 40 mm cover slips, Menzel-Gläser, Brunswick, Alemania), pretreated with iso-2-propanol, were treated with oxygen plasma for 30 s to surface activate the PDMS and promote glass-PDMS bonding. Sealed devices were incubated at 100 °C for 10 minutes then treated with 1 mg/mL poly-D-lysine (Sigma, St Louis, MO, United States) for one-channel devices or 0.01% w/v poly-L-lysine (Sigma, St Louis, MO, United States) for two-channel devices, for at least 1 hour at room temperature. Then, washed with deionized water, treated with 1 % glutaraldehyde for 15 min, and washed with deionized water for 24 hours on a shaker.

Formation of the Endothelial Vessel

After fabrication, bonding, and surface treatment, the devices were sterilized in a 70% ethanol solution for 30 minutes. A 0.16 mm diameter acupuncture needle (Φ 0.16 x 40 mm, Seirin, Shizuoka, Japan), pretreated with 0.01 % bovine serum albumin (BSA) in phosphate-buffered saline (PBS) for 30 min, was inserted into the device and sterilized with ultra violet light for 15 min. Subsequently, reconstituted type-I collagen derived from rat tail (Corning, Glendale, AZ, United States), was buffered to a pH of 7.5 with 1 N NaOH in sterile H₂O, 10x dPBS with phenol (Euroclone, Milan, Italy) and EGM-2 medium, was introduced in the central region of the device. Two different collagen concentrations were tested, 2.5 and 6 mg/mL, starting from stock concentrations at 4.33 and 9.44 mg/mL, respectively. Devices were moved to a humidified incubator at 37 °C for at least 2 h, and device reservoirs were filled of EGM-2 media to avoid dehydration of the hydrogel. Next, the needle was removed, and the device was sealed with vacuum grease (Millipore Sigma, Saint Louis, MO, United States). For two-channel devices, the same procedure was performed with two needles inserted into each device.

Fresh EGM-2 was introduced into devices, and devices were moved to a laboratory rocker within a humidified incubator to wash devices for 24 hrs. The next day, a HUVEC suspension with a final concentration of $2 \cdot 10^6$ cells/mL in EGM-2 was introduced into the device reservoirs, and cell adherence to the central channel in the collagen gel was observed by phase contrast microscopy Nikon D-Eclipse C1 Confocal Microscope, 10x lens, Nikon Instruments, Tokyo, Japan). As previously described, when the cylindrical space was covered by an adequate density of HUVECs [16], cell-containing media was replaced with fresh media and devices were incubated at 37 °C for 24 hours on a rocker at 30 degrees and 5 cycles/min to introduce oscillatory, reciprocating flow through the vessel lumen.

Extravasation Assays

For the extravasation assays, a solution of $7.5 \cdot 10^5$ cell/ml of THP-1 monocytes were resuspended in EGM-2 media and introduced into device ports. Devices were incubated at 37 °C for 24 hours prior to analysis (Fig. 1). To study the influence of flow in the extravasation process, devices were pretreated with oscillating flow for 24 hours before adding the monocytes, while static devices were maintained on a shelf of the same incubator **for 24 hours as well, prior to addition of monocytes**. To analyze the role of collagen density, extravasation assays were conducted with 2.5 and 6 mg/mL collagen hydrogels as described above.

Immunofluorescence

Devices were washed with PBS + 0.5 mM MgCl₂ + 1 mM CaCl₂ (PBS++), fixed with 4 % paraformaldehyde (PFA) at 37 °C for 20 min on the oscillatory rocker, and washed again with PBS++. Samples were permeabilized with 0.1 % Triton X (Calbiochem, Darmstadt, Alemania) for 20 minutes and washed with PBS++. Subsequently, devices were rocked with 4',6-diamino-2-fenilindol (DAPI) (1:1000) (Invitrogen, Carlsbad, CA, United States) and rhodamine phalloidin (1:200) (Thermo Fisher Scientific, Madrid, Spain) in 2 % BSA in PBS++ at room temperature for 20 min. After washing with 2 % BSA, devices were incubated with primary antibody against VE-cadherin (1:200) (Santa Cruz Biotechnology, Santa Cruz, CA, United States) in 2 % BSA in PBS++ at 4 °C overnight. Next, anti-goat Alexa Fluor 647 secondary antibody (1:250) (Thermo Fisher Scientific, Madrid, Spain) in 2% BSA in PBS++ was added at room temperature for 2 hours while protected from light. Finally, devices were washed with 2 % BSA and stored at 4 °C. Maximum intensity projections were synthesized from Z-stack series obtained with a laser scanning confocal microscopy (FV3000, Olympus) at 20x magnification (20x C Plan fluor 0.7 NA air objective, Olympus).

Image acquisition and analysis

Data for extravasation assays were obtained from the analysis of fixed immunofluorescence images taken as described above with a 20x objective. The number of extravasated and adhered monocytes, the monocyte migration distance, and diameters were measured manually using Fiji [50]. **Monocytes were identified and differentiated from HUVECs by their small size, rounded shape and different cell refractive index, which gave them a different shade of gray under the bright-field microscope [51], [52].**

Alignment of phalloidin and VE-cadherin networks was determined by analyzing the maximum intensity projection of seven independent assays. After the projection, vessel images were split in square patches and their walls were removed to avoid bias in the main direction of the vessel (Fig. S1). The alignment index (α) was estimated using a discrete Fourier Transform (FT) method as described previously [53], [54]. This index ranges from 0 to 1, with 1 meaning a complete alignment of the network and 0 a random orientation.

Permeability assays

Diffusive permeability of vessels was quantified as previously described [16]. Briefly, EGM-2 supplemented with 70-kDa fluorescent dextran TexasRed (200 µg/mL) (Sigma-Aldrich, Saint Louis, MO, United States) was introduced into the vessel, and images were taken at 10x magnification every 5 s for 50 cycles at the median transversal plane of the vessel. Total flux of dextran transported across the vascular wall was quantified by measuring the total intensity within the vessel for each time point (I_0), and the total intensity outside of the vessel

(I) as a function of time. The radius of the vessel (r), intensity within the vessel (I_0), and rate of change of intensity outside of the vessel ($\delta I/\delta t$) were used to determine P_d through the following relation:

$$P_d = \left(\frac{2r}{I_0}\right)\left(\frac{\delta I}{\delta t}\right)$$

Collagen hydrogel characterization

Collagen hydrogels at mass concentrations of 2.5 and 6 mg/mL were prepared as described above and frozen in liquid nitrogen overnight prior to lyophilization (ScanVac CoolSafe 110-4, Labogene, Lyngø, Denmark) for 44 hours. Samples were then deposited in holders on carbon tape and coated with a 14 nm layer of palladium to increase conductivity. The gels were visualized and photographed using a field scanning electron microscope (CSEM-FEG INSPECT F50, FEI Company, Hillboro, OR, United States) at resolutions of 10, 20, 50 and 100K.

Determination of hydraulic permeability

Following removal of needles in a two-channel device, all device reservoirs were emptied and filled with 70-kDa fluorescent dextran Fluorescein (FITC) (200 μ g/mL) (Sigma-Aldrich, Saint Louis, MO, United States) in PBS. These devices were then incubated overnight at 37 $^{\circ}$ C to allow the dextran to permeate the collagen hydrogel. The reservoirs were then emptied, and glass capillary tubes were inserted into the reservoirs of one channel. Any gaps between the PDMS and glass were sealed using vacuum grease, and the 70-kDa FITC solution was added to the glass reservoirs to apply a hydrostatic pressure of 5, 10, or 20 mmH₂O. Fluorescence recovery after photobleaching (FRAP) was performed by finding the median transversal plane of the vessel and photobleaching a 50 pixel circle in the collagen gel between the two channels for 3 seconds, followed by continuous imaging of the bleached circle every second for 30 seconds. The velocity of the interstitial flow induced by the hydrostatic pressure was calculated using a custom Matlab code that fit a circle to the bleached region and determined circle displacement across the time series.

RESULTS and DISCUSSION

Microfabricated blood vessels that mimic physiologic vasculature.

We fabricated a microfluidic cell culture system to develop microfabricated blood vessels, consisting of a perfusable channel lined with HUVECs embedded in 3D collagen hydrogel (Fig. 1). After seeding with endothelial cells, these devices were cultured with oscillatory flow or under static conditions for 24 hours. To characterize endothelial cell distribution within devices, we fixed the devices, stained them with DAPI, and performed a three-dimensional reconstruction of the spatial arrangement of the nuclei of endothelial cells forming the vessel (Fig. 2A). These reconstructions reveal a continuous cylindrical endothelial monolayer embedded within the collagen type I hydrogel. It has been shown previously that application of physiologic hemodynamic shear stress leads to alignment of the actin cytoskeleton [55]. To measure the alignment of filamentous actin fibers, we stained fixed devices with rhodamine phalloidin and anti-VE-cadherin antibodies. VE-cadherin is an adherent junction protein that in part regulates endothelial permeability [56], and assembly of VE-cadherin-containing junctions indicates the establishment of endothelial barrier function [57].

By performing a simple threshold segmentation of the VE-cadherin staining, we observed that all pixels were connected in a lattice of cell-cell junctions as a single object (Fig. 2B). This suggests that there are no gaps between the HUVECs forming the vessel and that it is in fact composed by a continuous monolayer of endothelial cells. We then computed an alignment index using a Fourier transform analysis of max intensity projections from z-stacks acquired with confocal microscopy. With this approach, we observed that the cytoskeleton presents an alignment index slightly greater than 0.5, and that VE-cadherin alignment was approximately 0.5. In both cases, there were no significant differences between vessels cultured under static and flow conditions (Fig. 2C). This index value indicates that the fibers are aligned mostly parallel to the vessel, in the same direction as flow. We further used devices stained with phalloidin to measure vessel diameter, which ranged from 125 to 250 μm (Fig. 2D) and is comparable to the diameter of human arterioles and venules [46], [47].

Fluid shear stress increases monocytes adherence to the vessel wall but decreases extravasation

Physiologically, fluid shear stresses stimulate monocytes and endothelial cells by increasing their expression of adhesion proteins, including E-selectin and ICAM-1, and by reorganizing the cytoskeleton of endothelial cells [12], [43]. To investigate the role of endothelial response to hemodynamic shear stress on monocyte attachment and extravasation, endothelial vessels were pretreated with 24 hours of oscillatory flow or were cultured in static conditions. After this differential treatment, monocytes were added to one of the reservoirs to introduce a hydrostatic pressure gradient resulting in flow of monocytes through the endothelial lumen for 24 hours.

Treatment of vessels with flow resulted an increase in adherent monocytes and a decrease in extravasated monocytes (Fig. 3A). To quantify this observation, monocyte nuclei stained with DAPI were counted in image stacks acquired with a laser-scanning confocal. Vessels pretreated with flow demonstrated between 5 and 20 adherent leukocytes per vessel (counted along the entire vessel), while static vessels did not exceed 10 monocytes per vessel (Fig. 3B). This statistically significant effect of flow is supported by previous work demonstrating that flow increases expression of proteins involved in monocyte adherence, including E-selectin and ICAM-1, in vascular endothelial cells [12]. Despite the increase in monocyte adherence to the lumen of flow-stimulated vessels, we found a decrease in the number of monocytes that traversed the endothelial barrier and migrated into the collagen hydrogel. As quantified from confocal z-stacks, extravasated monocytes in static vessels ranged from 5 to 20 per vessel, whereas when treated with flow, the range is reduced to 1 to 10 (Fig. 3C). We hypothesized that the decreased rate of extravasation could be due to the effects of flow on vascular endothelial barrier integrity, as permeability of endothelial cell monolayers decreases with applied flow [43].

To test this hypothesis and to determine whether flow impacts barrier function of the vascular endothelial monolayer, we quantified the diffusive flux of fluorescently tagged 70 kDa dextran from the vessel lumen into the hydrogel using time lapse confocal microscopy. After 100 seconds of dextran perfusion, we observed a stark difference between the distribution of dextran throughout the hydrogels, with the levels of dextran within the subluminal matrix nearly equivalent to those in the lumen for vessels cultured in static conditions (Fig. 3D). To quantify this observation, we measured the diffusive permeability of vessels, a measure of the barrier to diffusive flux in response to discrete changes in concentration across a

membrane, in this case the endothelial monolayer. We found a significant difference in the diffusive permeability of vessels cultured in static vs. flow conditions, with the mean permeability more than 10 times higher in static vessels (mean = 1.45 $\mu\text{m/s}$) than in flow-treated vessels (mean = 0.10 $\mu\text{m/s}$) (Fig. 3E), consistent with previous observations [58]. Previous work has demonstrated that a flow-mediated reduction in vascular permeability is driven by the assembly of VE-cadherin-containing adherens junction complexes [17], and we hypothesize that this junctional assembly presents a barrier to monocyte migration and extravasation. This hypothesis is further supported by work demonstrating that VE-cadherin expression levels are increased with flow [59] and is an essential part of a mechanosensory complex that plays a role in the establishment and maturation of tight junctions [60], [61], and that mature adherens junctions present a barrier to monocyte extravasation [3].

Interestingly, once monocytes have crossed the endothelial barrier, there is no difference in the total migration distance through the collagen gel. In both conditions, monocytes travel around 20 μm from the vessel wall (Fig. 3F). These results are similar to previously published data by Boussommier-Calleja *et al.*, which indicated that after extravasation, monocytes tended to migrate between 10-20 μm [62]. Our longer migration distances might be explained by differences in the hydrogels used. Boussommier-Calleja worked with 3 mg/mL fibrin collagens, whereas we use 2.5 mg/mL collagen gels. In addition, fibrin gels present different fiber organization, with smaller pore sizes [63]. It has also been demonstrated that cells encounter greater steric hindrance in their advance and migrate shorter distances when traversing fibrin gels compared to collagen gels [64].

Increased collagen matrix concentration decreases vascular barrier integrity and increases extravasation

The physical properties of the endothelial basement membrane and intimal tissue are known to modulate vascular barrier function and inflammation [65]. Previous work demonstrated that increased intimal stiffness results in increased vascular permeability and immune cell extravasation through activation of Rho-mediated contractility in endothelial cells [66]. To elucidate the role of collagen matrix concentration on permeability and extravasation in our microfluidic model, we synthesized vessels in 2.5 and 6 mg/mL collagen type I hydrogels. It has been previously demonstrated that a change in collagen concentration impacts the biophysical properties of hydrogels. Our group previously analyzed the storage shear modulus (G'), which indicates the elastic response of a material to shear stress, as a function of collagen mass concentration. We found that 2.5 mg/mL hydrogels were characterized by a G' of 62.14 ± 4.87 Pa, while 6 mg/mL hydrogels were characterized by a G' of 254.05 ± 29.06 Pa (Fig. S2) [67]. Oliveros *et al.* performed a computational spatial characterization of the collagen fibers that comprise the solid phase of the hydrogel, and determined that increasing collagen concentration resulted in a decrease in pore size and porosity of the material. In addition, they found that increasing collagen concentration resulted in an increase in the number of fibers, while the length and radius of the fibers decreased [68]. We examined the structure of collagen hydrogels with SEM (Fig. 4A). Consistent with previous results, at lower magnifications, we found that the 2.5 mg/mL hydrogels by increased void space when compared to the 6 mg/mL hydrogels, and increased suggests the 6 mg/mL gels are comprised of thicker fibers with more junctions between fibers (Fig. 4A). Together these data indicate that the increase in collagen concentration results in changes in the spatial distribution of collagen fibers, which we expect to impact mechanical

properties. To determine whether these structural differences presented differential functional barriers to migration, we determined the hydraulic permeability, which is related to the effective pore size. The hydraulic permeability of the different collagen compositions was determined by applying a hydrostatic pressure of 5, 10, or 20 mmH₂O using 70-kDa FITC dextran across a two-channel device and measuring the resulting velocity across the collagen between the two channels (Fig. 4B). FRAP was performed by photobleaching a spot between the channels and imaging the displacement of the circle over time (Fig. 4C). This displacement was used to calculate the velocity of fluid (Fig. 4D) due to the applied hydrostatic pressures and used to calculate the hydraulic permeability in each condition, and statistically significant decreases in hydraulic permeability were found between the two hydrogel compositions (Fig. 4E).

To determine the impact of collagen concentration on vascular barrier function and monocyte extravasation, we repeated the diffusive permeability assay in vessels synthesized in 2.5 mg/mL vs. 6 mg/mL collagen hydrogels and exposed to flow. Increased collagen concentration resulted in significant increases in vascular permeability (Fig. 5A). Quantitatively, the average permeability in high collagen concentration gels (mean = 0.60 $\mu\text{m/s}$) is six times higher than the mean obtained in lower collagen concentration gels (mean = 0.10 $\mu\text{m/s}$). In 2.5 mg/mL gels, the permeability ranges from 0 to 0.2 $\mu\text{m/s}$, while in 6 mg/mL gels, it ranges from 0.1 to almost 0.9 $\mu\text{m/s}$ (Fig. 5B). Interestingly, despite the decreased pore size of the 6 mg/mL collagen gels, there were nearly twice as many extravasated monocytes in the 6 mg/mL hydrogels compared to the 2.5 mg/mL hydrogels. (Fig. 5C). Our data suggest that the integrity of endothelial vessels plays an essential role in monocyte extravasation, and is more impactful than the steric hindrance caused by the higher collagen concentrations.

CONCLUSIONS

Here, we introduce a microfluidic model of a monocyte-laden perfusable 3D blood vessel and demonstrate the ability to recapitulate monocyte arrest, extravasation, and 3D migration through a subluminal matrix. Importantly, this model system improves upon traditional assays by allowing for modulation of key hemodynamic parameters, including pressure and flow, for vessels embedded within a three-dimensional extracellular matrix with varying density. We demonstrate that both flow and matrix density play key roles in adhesion, extravasation, and migration, and interestingly, our data demonstrate a complex interplay among biophysical parameters that govern monocyte-endothelial interactions. While flow promotes adhesion of monocytes to the vascular wall, the number of cells that extravasate into the subluminal matrix decreases with flow, suggesting that extravasation, rather than adhesion, is the rate limiting step for immune cell trafficking in the presence of flow. This idea is supported by vascular permeability data, which demonstrates increased barrier to diffusion of 70 kDa dextran in the presence of flow, and further suggests that targeting vascular permeability could be an effective strategy for screening the passage of molecules or other cells through the endothelial wall, such as drugs that must diffuse to their target organ or pathogen, or metastatic cells in cancer progression.

Devices fabricated in a similar manner, by casting a hydrogel around a needle to ultimately form a perfusable vessel embedded within a 3D hydrogel, have been used for numerous

applications to study the impact of the biochemical and biophysical microenvironment on microvascular morphogenesis and function. Such devices have been implemented to screen the effects of pro-angiogenic cocktails on neovascularization [69], to define the role of matrix degradability in angiogenesis [70], and to determine the role of inflammatory factors in governing lymphatic drainage [71]. Yet, in most of these studies (reviewed in [72]), cell culture media is used as a blood surrogate, and the contributions of circulating cells towards microvessel function are not considered, despite increasing evidence that leukocytes and immune cells play critical roles in microvascular development, homeostasis, and dysfunction [73]. Our results demonstrate that such platforms are compatible with circulating cells and suggest that mechanistic studies enabled by these devices could allow for dissection of key signals involved in pathologies such as fibrosis and cancer, where changes in ECM composition and mechanics occur concomitantly with changes in hemodynamics, to identify and screen therapeutic interventions. **One challenge in the use of the current device for drug screening or other applications requiring a large number of devices is the overall time required to fabricate and conduct studies in the device proposed here (>72hrs from pouring PDMS to introducing monocytes). Much of this time (48hrs) is spent washing the device to prevent glutaraldehyde-induced cytotoxicity. Recently, dopamine hydrochloride has been demonstrated as an alternative surface coating to glutaraldehyde that is much less cytotoxic and does not require such substantial washing [49]. The use of dopamine hydrochloride could remove 48hrs from our fabrication protocol and reduce the device assembly process to something that can easily be completed within one day.**

While the application of flow impacted the rate of monocyte adherence and extravasation, the migration distance of monocytes into the collagen hydrogel was not dependent on the application of flow. Given that tissues demonstrate varying degrees of infiltration by monocytes and other circulating cells *in vivo*, it is likely that the platform described here does not recapitulate sufficient complexity to investigate mechanisms that lead to differences in cell migration behaviors beyond extravasation. **By focusing only on the adhesion and extravasation process, we do not recapitulate some key cellular events that occur before and after the extravasation and that may influence the final outcome of monocyte or immune cell surveillance. The addition of chemical and biological stimuli from perivascular tissue, such as chemokines or molecules derived from microorganisms, would allow the study of the recruitment of monocytes to damaged tissue [8] and subsequent differentiation into macrophages in the extracellular matrix [74], [75]. In this way, a more complete and physiologic model could be achieved. The introduction of perivascular signals and gradients will be the focus of future studies, as the lateral ports of the device described here (Fig. 1) provide access to hydrogel tissue region and can be used to establish molecular or pressure gradients.** Furthermore, recent work introducing epithelial ducts into lumenized vascular devices [76] and coculturing diverse bacterial colonies on chip [77] together illustrate the potential to recapitulate complex inflammatory responses *in vitro* through the integration of these approaches.

SUPPLEMENTAL MATERIAL

See **Supplemental Material** for details on computational image processing, hydrogel stiffness data, and analysis of correlations between vessel properties and monocyte extravasation.

This is the author's peer reviewed, accepted manuscript. However, the online version of record will be different from this version once it has been copyedited and typeset.
PLEASE CITE THIS ARTICLE AS DOI: 10.1063/5.0061997

AUTHOR'S CONTRIBUTIONS

S.P.-R. and W.J.P. conceived of the experiments. S.P.-R. conducted experiments involving monocytes and measures of vascular phenotype and permeability, and S.A.H. conducted hydraulic permeability measurements. S.P.-R., S.A.H., and C.B. processed data and prepared figures. S.P.-R., S.A.H., and C.B. wrote the manuscript, which was edited by J.M.G.A. and W.J.P.

ACKNOWLEDGEMENTS

This work was supported by the Spanish Ministry of Education, Culture and Sport (FPU grant: FPU16/04398) to S. P.-R., the Spanish Ministry of Science, Innovation and Universities (RTI2018-094494-B-C21) to J. M. G. A, and the US National Institutes of Health (T32HL69768, S.A.H.). This work was performed in part at the Chapel Hill Analytical and Nanofabrication Laboratory, CHANL, a member of the North Carolina Research Triangle Nanotechnology Network, RTNN, which is supported by the National Science Foundation (ECCS-2025064), as part of the National Nanotechnology Coordinated Infrastructure, NNCI.

Authors would like to acknowledge the use of Servicio General de Apoyo a la Investigación-SAI, Universidad de Zaragoza.

AUTHOR DECLARATIONS

Conflict of Interest

The authors have no conflicts to disclose.

DATA AVAILABILITY

The data that support the findings of this study are available from the corresponding author upon reasonable request.

This is the author's peer reviewed, accepted manuscript. However, the online version of record will be different from this version once it has been copyedited and typeset.
 PLEASE CITE THIS ARTICLE AS DOI: 10.1063/5.0061997

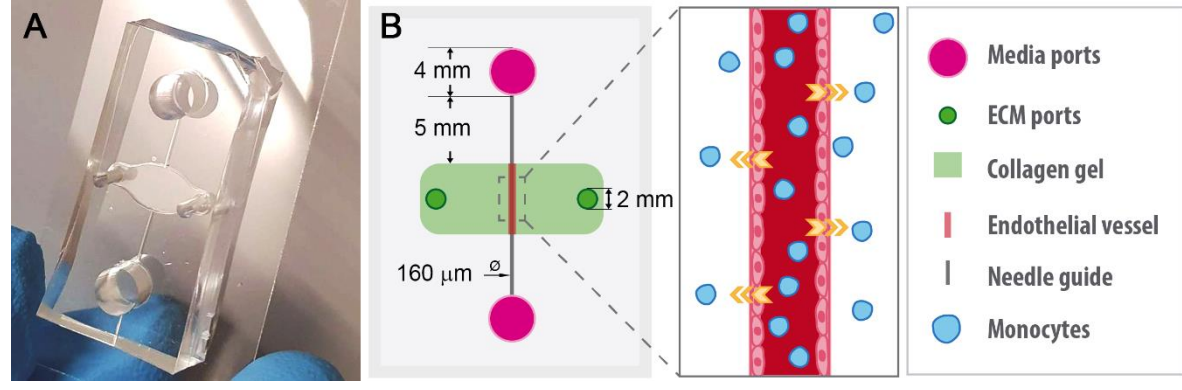


Figure 1. Microfluidic platform for investigating monocyte extravasation. A) Photograph of device bonded to (24 mm x 40 mm coverslip). B) Graphical representation of the device (not to scale) that consists of a central chamber with two ports (dark green) through which the collagen gel (light green) is introduced and polymerized. A channel formed by an acupuncture needle connects two reservoirs filled with medium (bright pink) to the collagen gel region. HUVECs line the channel in the collagen gel (pink), and hydrostatic pressure gradients induced by the rocker induce flow through the channel. Monocytes (blue) are flowed through the vessel, and extravasation from the lumen into the collagen hydrogel is investigated using light microscopy.

This is the author's peer reviewed, accepted manuscript. However, the online version of record will be different from this version once it has been copyedited and typeset.
PLEASE CITE THIS ARTICLE AS DOI: 10.1063/5.0061997

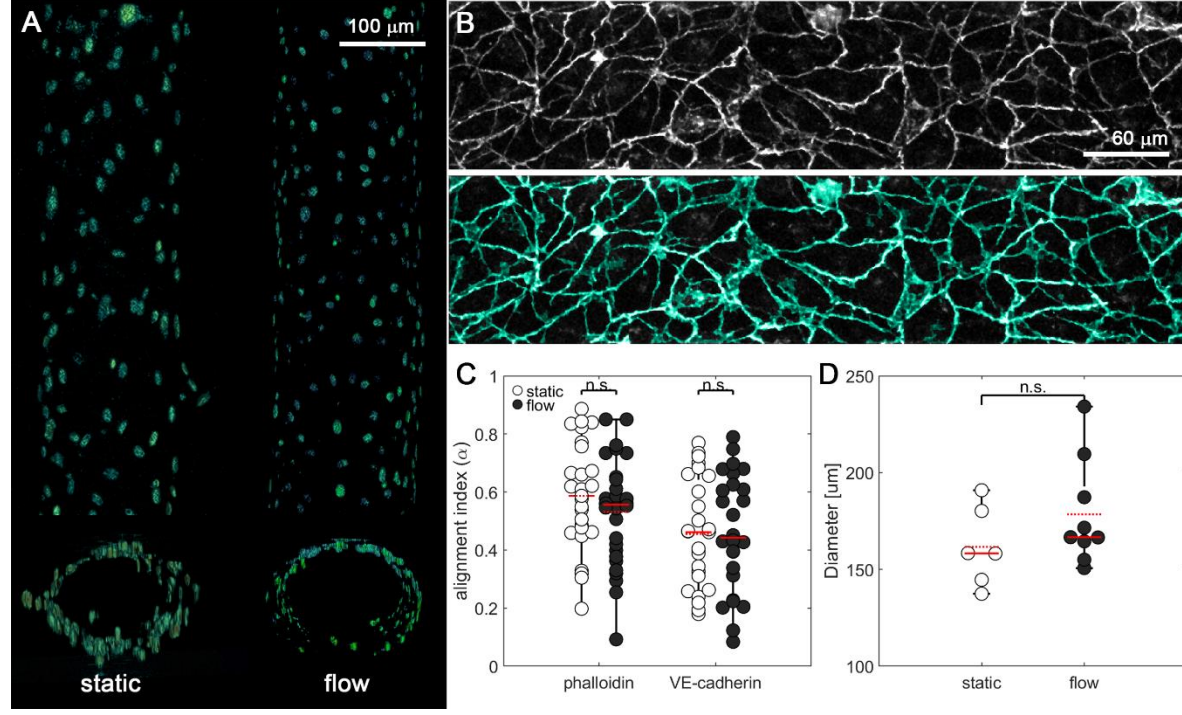


Figure 2. Endothelial vessels embedded in 2.5 and 6 mg/mL collagen gels within the microfluidic device. A) Three-dimensional reconstruction from nuclei staining with DAPI, showing a longitudinal (upper) and transverse (lower) view from a static and a flow vessel. B) First row shows a grayscale example of the VE-cadherin staining of a vessel (maximum intensity projection) while second row shows, superimposed in cyan, the segmentation of the former performed by simple thresholding. C) Phalloidin and VE-cadherin alignment index (α) of the maximum fluorescence projection of an endothelial vessel, with 1 being the complete alignment parallel to the vessel. D) Diameters of each static and flow endothelial vessel. For all plots, each data point represents data from an individual device, and solid and dashed red lines represent the median and mean values, respectively. ANOVA tests were performed to determine statistical significance. * $p < 0.05$.

This is the author's peer reviewed, accepted manuscript. However, the online version of record will be different from this version once it has been copyedited and typeset.
 PLEASE CITE THIS ARTICLE AS DOI: 10.1063/5.0061997

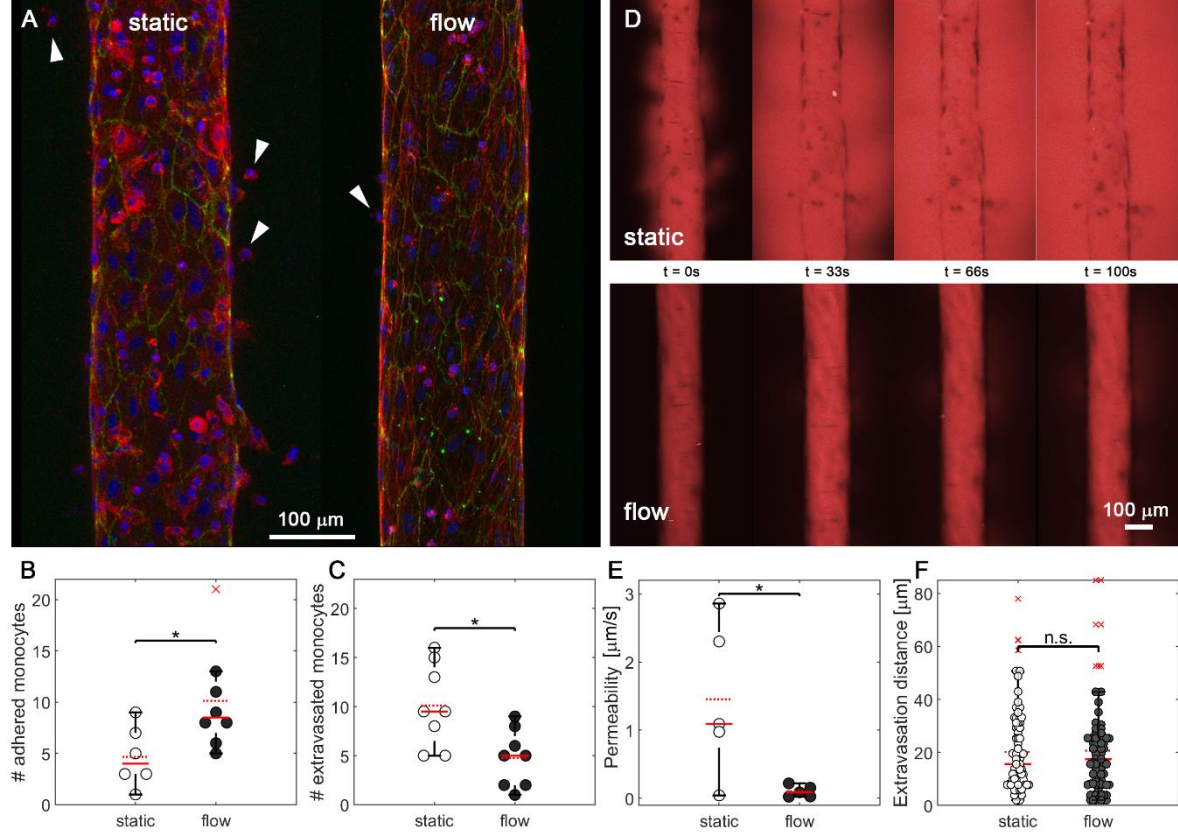


Figure 3. Effect of the fluid flow stimulation on extravasation. A) Endothelial vessels in 2.5 mg/mL hydrogels in static (left) and flow-pretreated (right) conditions. Vessels are stained for actin (red), VE-cadherin (green) and nucleus (blue). Extravasated monocytes are indicated with white arrows. B) Number of monocytes adhered to the endothelial lumen in static (white) and flow-pretreated (black) vessels. C) Number of monocytes extravasated from the lumen to the surrounding hydrogel in static (white) and flow-pretreated (black) vessels. D) Permeability assay with 70 kDa fluorescent dextran (red) added to the endothelial lumen. Images are single confocal slices taken after the addition of dextran in a static (upper) and a flow-pretreated (lower) vessel. E) Permeability of static (white) and flow-pretreated (black) vessels. F) Distance migrated by monocytes from the endothelial wall to the collagen gel in static (white) and flow-pretreated (black) vessels. For all plots, each data point represents data from an individual device, solid and dashed red lines represent the median and mean values, respectively. Red crosses represent outliers. ANOVA tests were performed to determine statistical significance. * $p < 0.05$.

This is the author's peer reviewed, accepted manuscript. However, the online version of record will be different from this version once it has been copyedited and typeset.
 PLEASE CITE THIS ARTICLE AS DOI: 10.1063/5.0061997

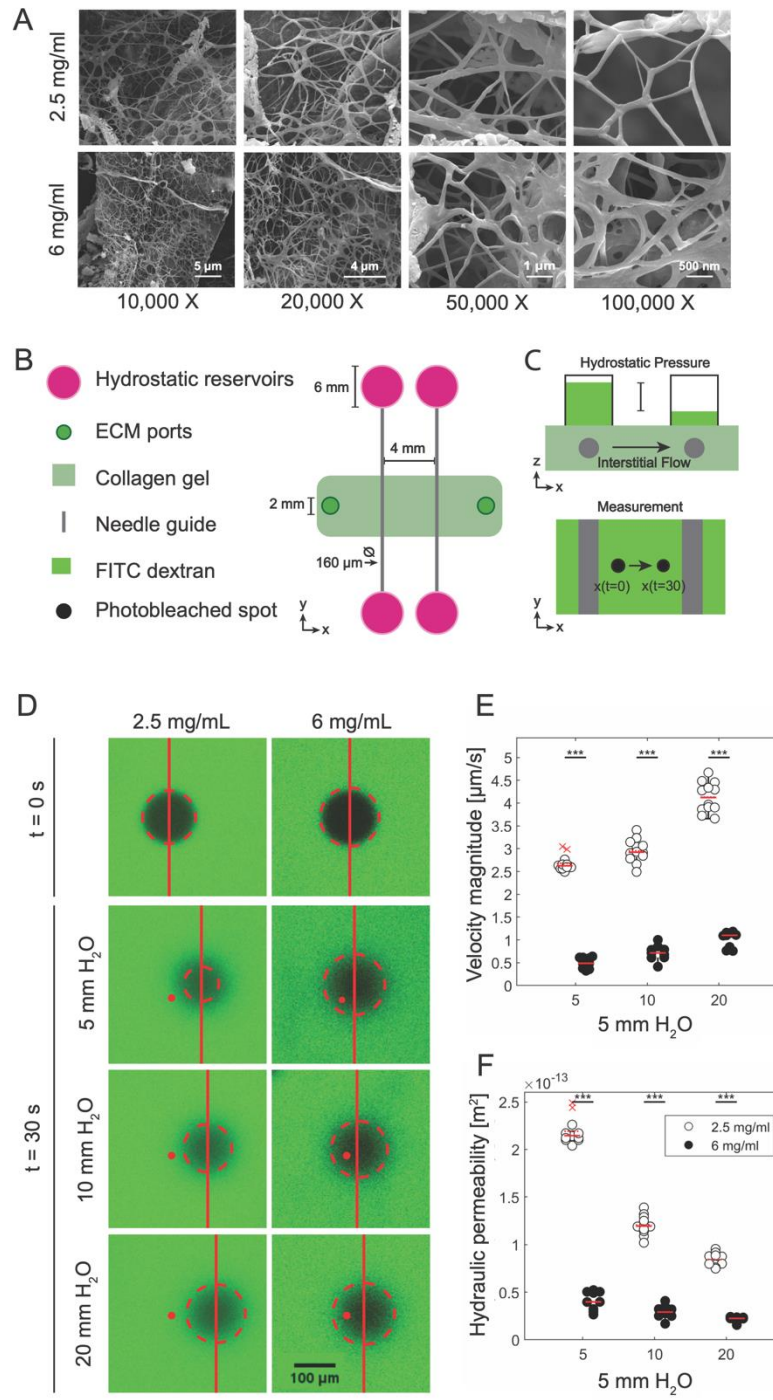


Figure 4. 3D structure and hydraulic permeability of 2.5 and 6 mg/mL collagen gels. A) Scanning electron microscope (SEM) images of 2.5 mg/mL and 6 mg/mL gels at resolutions of 10, 20, 50 and 100K. B) Diagram of two-channel device used to measure hydraulic permeability. Reservoirs are connected to the media ports to allow application of a defined pressure gradient across the collagen hydrogel. C) Experimental setup of fluorescence recovery after photobleaching (FRAP) method used to measure the hydraulic permeability. A known pressure gradient is applied to hydrogels immersed in dextran-containing medium, and the velocity magnitude of a photobleached circle is measured with timelapse

This is the author's peer reviewed, accepted manuscript. However, the online version of record will be different from this version once it has been copyedited and typeset.

PLEASE CITE THIS ARTICLE AS DOI: 10.1063/5.0061997

fluorescence microscopy. D) Sample FRAP data demonstrating spot displacement in response to an applied hydrostatic pressure gradient. E) Measured velocity of fluid flow between two channels. F) Hydraulic permeability of collagen hydrogels as a function of applied pressure gradient calculated from Darcy's law. For all plots, each data point represents data from an individual device, solid and dashed red lines represent the median and mean values, respectively. ANOVA tests were performed to determine statistical significance. *** $p < 0.001$.

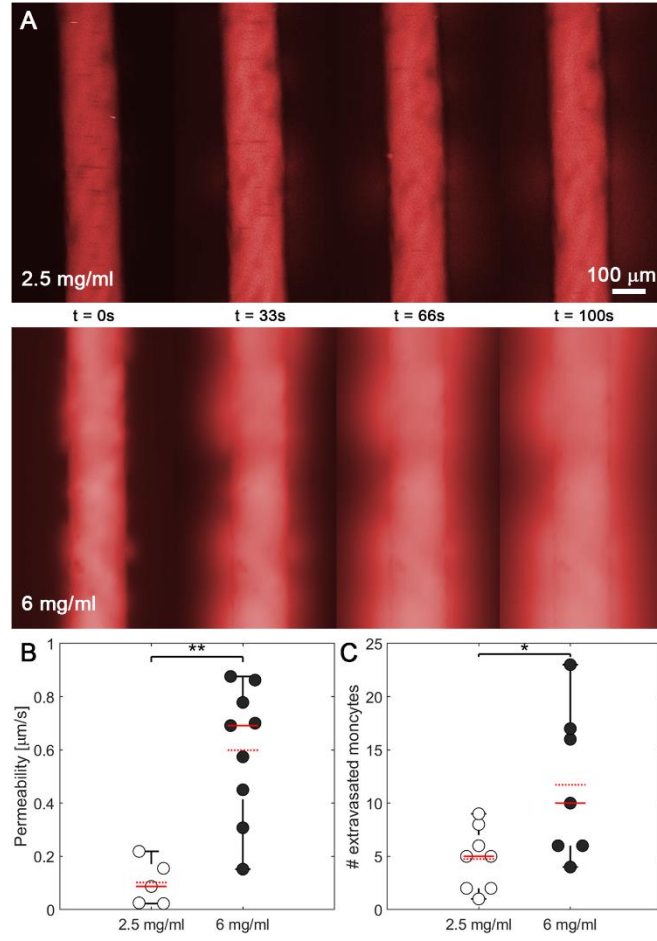


Figure 5. Effect of the collagen concentration on vascular permeability and monocyte extravasation. A) Diffusive permeability assay with fluorescent dextran (red) diffusing from the vessel lumen through the endothelial monolayer at different times ($t= 0, 33, 66,$ and 100 seconds) in vessels formed in 2.5 mg/mL (upper) and 6 mg/mL collagen hydrogels (lower). B) Diffusive permeability of vessels embedded in 2.5 mg/mL (white) and 6 mg/mL collagen hydrogels (black). C) Number of monocytes extravasated from the lumen into the surrounding hydrogel in 2.5 mg/mL (white) 6 mg/mL collagen hydrogels (black). For all plots, each data point represents data from an individual device, solid and dashed red lines represent the median and mean values, respectively. ANOVA tests were performed to determine statistical significance. * $p < 0.01$; ** $p < 0.05$.

REFERENCES

- [1] I. Goutos, L. K. Cogswell, and H. Giele, "Extravasation injuries: A review," *J. Hand Surg. Eur. Vol.*, vol. 39, no. 8, pp. 808–818, 2014, doi: 10.1177/1753193413511921.
- [2] N. Reglero-Real, D. García-Weber, and J. Millán, "Cellular Barriers after Extravasation: Leukocyte Interactions with Polarized Epithelia in the Inflamed Tissue," *Mediators Inflamm.*, vol. 2016, 2016, doi: 10.1155/2016/7650260.
- [3] T. Gerhardt and K. Ley, "Monocyte trafficking across the vessel wall," *Cardiovasc. Res.*, vol. 107, no. 3, pp. 321–330, 2015, doi: 10.1093/cvr/cvv147.
- [4] N. Wettschureck, B. Strilic, and S. Offermanns, "Passing the vascular barrier: Endothelial signaling processes controlling extravasation," *Physiol. Rev.*, vol. 99, no. 3, pp. 1467–1525, 2019, doi: 10.1152/physrev.00037.2018.
- [5] J.-K. Min *et al.*, "TNF-Related Activation-Induced Cytokine Enhances Leukocyte Adhesiveness: Induction of ICAM-1 and VCAM-1 via TNF Receptor-Associated Factor and Protein Kinase C-Dependent NF- κ B Activation in Endothelial Cells," *J. Immunol.*, vol. 175, no. 1, pp. 531–540, 2005, doi: 10.4049/jimmunol.175.1.531.
- [6] W. Y. Hsu *et al.*, "Resistin induces monocyte-endothelial cell adhesion by increasing ICAM-1 and VCAM-1 expression in endothelial cells via p38MAPK-dependent pathway," *J. Cell. Physiol.*, vol. 226, no. 8, pp. 2181–2188, 2011, doi: 10.1002/jcp.22555.
- [7] B. Schmitz *et al.*, "Increased monocyte adhesion by endothelial expression of VCAM-1 missense variation invitro," *Atherosclerosis*, vol. 230, no. 2, pp. 185–190, 2013, doi: 10.1016/j.atherosclerosis.2013.07.039.
- [8] B. León and C. Ardavín, "Monocyte migration to inflamed skin and lymph nodes is differentially controlled by L-selectin and PSGL-1," *Blood*, vol. 111, no. 6, pp. 3126–3130, 2008, doi: 10.1182/blood-2007-07-100610.
- [9] S. M. Dudek and J. G. N. Garcia, "Cytoskeletal regulation of pulmonary vascular permeability," *J. Appl. Physiol.*, vol. 91, pp. 1487–1500, 2001, doi: 10.1016/j.envpol.2004.10.021.
- [10] M. B. Voisin, A. Woodfin, and S. Nourshargh, "Monocytes and neutrophils exhibit both distinct and common mechanisms in penetrating the vascular basement membrane in vivo," *Arterioscler. Thromb. Vasc. Biol.*, vol. 29, no. 8, pp. 1193–1199, 2009, doi: 10.1161/ATVBAHA.109.187450.
- [11] A. R. Schenkel, Z. Mamdouh, and W. A. Muller, "Locomotion of monocytes on endothelium is a critical step during extravasation," *Nat. Immunol.*, vol. 5, no. 4, pp. 393–400, 2004, doi: 10.1038/ni1051.
- [12] M. P. Burns and N. DePaola, "Flow-conditioned HUVECs support clustered leukocyte adhesion by coexpressing ICAM-1 and E-selectin," *Am. J. Physiol. - Hear. Circ. Physiol.*, vol. 288, no. 1 57-1, pp. 194–204, 2005, doi: 10.1152/ajpheart.01078.2003.
- [13] D. C. Chappell, S. E. Varner, R. M. Nerem, R. M. Medford, and R. W. Alexander, "Expression in Cultured Human Endothelium," *Circ. Res.*, vol. 82, pp. 532–539, 1998.

This is the author's peer reviewed, accepted manuscript. However, the online version of record will be different from this version once it has been copyedited and typeset.
PLEASE CITE THIS ARTICLE AS DOI: 10.1063/1.50061997

- [14] R. S. Gonzales and T. M. W. Ph.D., "Hemodynamic modulation of monocytic cell adherence to vascular endothelium," *Ann. Biomed. Eng.*, vol. 24, pp. 382–393, 1996.
- [15] E. Tzima *et al.*, "Activation of Rac1 by shear stress in endothelial cells mediates both cytoskeletal reorganization and effects on gene expression," *EMBO J.*, vol. 21, no. 24, pp. 6791–6800, 2002.
- [16] W. J. Polacheck, M. L. Kutys, J. B. Tefft, and C. S. Chen, *Microfabricated blood vessels for modeling the vascular transport barrier*, vol. 14, no. 5. Springer US, 2019.
- [17] W. J. Polacheck *et al.*, "A non-canonical Notch complex regulates adherens junctions and vascular barrier function," *Nature*, vol. 552, no. 7684, pp. 258–262, 2017, doi: 10.1038/nature24998.
- [18] J. D. Humphrey, E. R. Dufresne, and M. A. Schwartz, "Mechanotransduction and extracellular matrix homeostasis," *Nat Rev Mol Cell Biol.*, vol. 15, no. 12, pp. 802–812, 2014, doi: 10.1038/nrm3896.
- [19] A. Mammoto *et al.*, "Control of lung vascular permeability and endotoxin-induced pulmonary oedema by changes in extracellular matrix mechanics," *Nat. Commun.*, vol. 4, 2013, doi: 10.1038/ncomms2774.
- [20] J. L. MacKaya and D. A. Hammer, "Stiff substrates enhance monocytic cell capture through Eselectin but not P-selectin," *Integr Biol*, vol. 8, no. 1, pp. 62–72, 2016, doi: 10.1039/c5ib00199d.
- [21] L. Schimmel *et al.*, "Stiffness-Induced Endothelial DLC-1 Expression Forces Leukocyte Spreading through Stabilization of the ICAM-1 Adhesome," *Cell Rep.*, vol. 24, no. 12, pp. 3115–3124, 2018, doi: 10.1016/j.celrep.2018.08.045.
- [22] K. A. Dzenko, A. V. Andjelkovic, W. A. Kuziel, and J. S. Pachter, "The chemokine receptor CCR2 mediates the binding and internalization of monocyte chemoattractant protein-1 along brain microvessels," *J. Neurosci.*, vol. 21, no. 23, pp. 9214–9223, 2001, doi: 10.1523/jneurosci.21-23-09214.2001.
- [23] R. E. Gerszten *et al.*, "MCP-1 and IL-8 trigger firm adhesion of monocytes to vascular endothelium under flow conditions," *Nature*, vol. 398, no. 6729, pp. 718–725, 1999, doi: 10.1038/19546.
- [24] Y. Sawa and E. Tsuruga, "The expression of E-selectin and chemokines in the cultured human lymphatic endothelium with lipopolysaccharides," *J. Anat.*, vol. 212, no. 5, pp. 654–663, 2008, doi: 10.1111/j.1469-7580.2008.00892.x.
- [25] Z. Brown, M. E. Gerritsen, W. W. Carley, R. M. Strieter, S. L. Kunkel, and J. Westwick, "Chemokine gene expression and secretion by cytokine-activated human microvascular endothelial cells: Differential regulation of monocyte chemoattractant protein-1 and interleukin-8 in response to interferon- γ ," *Am. J. Pathol.*, vol. 145, no. 4, pp. 913–921, 1994.
- [26] B. J. Rollins and J. S. Pober, "Interleukin-4 induces the synthesis and secretion of MCP-1/JE by human endothelial cells," *Am. J. Pathol.*, vol. 138, no. 6, pp. 1315–1319, 1991.
- [27] J. Middleton *et al.*, "Transcytosis and surface presentation of IL-8 by venular

- endothelial cells," *Cell*, vol. 91, no. 3, pp. 385–395, 1997, doi: 10.1016/S0092-8674(00)80422-5.
- [28] W. A. Muller, "Mechanisms of Leukocyte Transendothelial Migration," *Annu Rev Pathol*, vol. 6, pp. 323–344, 2011, doi: 10.1161/CIRCULATIONAHA.110.956839.
- [29] J. Middleton, A. M. Patterson, L. Gardner, C. Schmutz, and B. A. Ashton, "Leukocyte extravasation: Chemokine transport and presentation by the endothelium," *Blood*, vol. 100, no. 12, pp. 3853–3860, 2002, doi: 10.1182/blood.V100.12.3853.
- [30] J. Escribano *et al.*, "Balance of mechanical forces drives endothelial gap formation and may facilitate cancer and immune-cell extravasation," *PLoS Comput. Biol.*, vol. 15, no. 5, pp. 1–21, 2019, doi: 10.1371/journal.pcbi.1006395.
- [31] E. L. Doherty, W. Y. Aw, A. J. Hickey, and W. J. Polacheck, "Microfluidic and Organ-on-a-Chip Approaches to Investigate Cellular and Microenvironmental Contributions to Cardiovascular Function and Pathology," *Front. Bioeng. Biotechnol.*, vol. 9, no. February, pp. 1–14, 2021, doi: 10.3389/fbioe.2021.624435.
- [32] R. Molteni *et al.*, "A novel device to concurrently assess leukocyte extravasation and interstitial migration within a defined 3D environment," *Lab Chip*, vol. 15, no. 1, pp. 195–207, 2015, doi: 10.1039/c4lc00741g.
- [33] S. Bersini, J. S. Jeon, M. Moretti, and R. D. Kamm, "In vitro models of the metastatic cascade: from local invasion to extravasation," *Drug Discov Today*, vol. 19, no. 6, pp. 735–742, 2014, doi: 10.1038/jid.2014.371.
- [34] H. K. Song and D. Y. Hwang, "Use of C57BL/6N mice on the variety of immunological researches," *Lab. Anim. Res.*, vol. 33, no. 2, pp. 119–123, 2017, doi: 10.5625/lar.2017.33.2.119.
- [35] W. A. Muller, "Getting Leukocytes to the Site of Inflammation," *Vet Pathol*, vol. 50, no. 1, pp. 7–22, 2013, doi: 10.1038/jid.2014.371.
- [36] B. K. Gale *et al.*, "A review of current methods in microfluidic device fabrication and future commercialization prospects," *Inventions*, vol. 3, no. 3, 2018, doi: 10.3390/inventions3030060.
- [37] E. K. Sackmann, A. L. Fulton, and D. J. Beebe, "The present and future role of microfluidics in biomedical research," *Nature*, vol. 507, no. 7491, pp. 181–189, 2014, doi: 10.1038/nature13118.
- [38] H. Xu *et al.*, "A dynamic in vivo-like organotypic blood-brain barrier model to probe metastatic brain tumors," *Sci. Rep.*, vol. 6, no. November, pp. 1–12, 2016, doi: 10.1038/srep36670.
- [39] J. S. Jeon *et al.*, "Human 3D vascularized organotypic microfluidic assays to study breast cancer cell extravasation," *Proc. Natl. Acad. Sci. U. S. A.*, vol. 112, no. 1, pp. 214–219, 2015, doi: 10.1073/pnas.1417115112.
- [40] S. Bersini *et al.*, "A microfluidic 3D invitro model for specificity of breast cancer metastasis to bone," *Biomaterials*, vol. 35, no. 8, pp. 2454–2461, 2014, doi: 10.1016/j.biomaterials.2013.11.050.
- [41] Y.-H. V. Ma, K. Middleton, L. You, and Y. Sun, "A review of microfluidic approaches

- for investigating cancer extravasation during metastasis," *Microsystems Nanoeng.*, vol. 4, no. 17104, 2018, doi: 10.1038/micronano.2017.104.
- [42] C. Kühnbach, S. da Luz, F. Baganz, V. C. Hass, and M. M. Mueller, "A microfluidic system for the investigation of tumor cell extravasation," *Bioengineering*, vol. 5, no. 2, 2018, doi: 10.3390/bioengineering5020040.
- [43] E. Bianchi, R. Molteni, R. Pardi, and G. Dubini, "Microfluidics for in vitro biomimetic shear stress-dependent leukocyte adhesion assays," *J. Biomech.*, vol. 46, no. 2, pp. 276–283, 2013, doi: 10.1016/j.jbiomech.2012.10.024.
- [44] S. Bersini *et al.*, "A combined microfluidic-transcriptomic approach to characterize the extravasation potential of cancer cells," *Oncotarget*, vol. 9, no. 90, pp. 36110–36125, 2018, doi: 10.18632/oncotarget.26306.
- [45] C. Frantz, K. M. Stewart, and V. M. Weaver, "The extracellular matrix at a glance," *J. Cell Sci.*, vol. 123, no. 24, pp. 4195–4200, 2010, doi: 10.1242/jcs.023820.
- [46] C. M. Jones *et al.*, "Measurement science in the circulatory system," *Cell. Mol. Bioeng.*, vol. 7, no. 1, pp. 1–14, 2014, doi: 10.1007/s12195-013-0317-4.
- [47] S. Ricci, "Anatomy," in *Sclerotherapy*, 2017, pp. 1–16.
- [48] P. Daniel Harris, BA, Lynn McNicoll, MD, Gary Epstein-Lubow, MD, and Kali S. Thomas, "Vessel sampling and blood flow velocity distribution with vessel diameter for characterizing the human bulbar conjunctival microvasculature," *Physiol. Behav.*, vol. 176, no. 1, pp. 139–148, 2017, doi: 10.1016/j.physbeh.2017.03.040.
- [49] S. E. Park, A. Georgescu, J. M. Oh, K. W. Kwon, and D. Huh, "Polydopamine-Based Interfacial Engineering of Extracellular Matrix Hydrogels for the Construction and Long-Term Maintenance of Living Three-Dimensional Tissues," *ACS Appl. Mater. Interfaces*, vol. 11, no. 27, pp. 23919–23925, 2019, doi: 10.1021/acsami.9b07912.
- [50] J. Schindelin *et al.*, "Fiji - an Open platform for biological image analysis," *Nat. Methods*, vol. 9, no. 7, 2019, doi: 10.1038/nmeth.2019.Fiji.
- [51] P. Y. Liu *et al.*, "Cell refractive index for cell biology and disease diagnosis: Past, present and future," *Lab Chip*, vol. 16, no. 4, pp. 634–644, 2016, doi: 10.1039/c5lc01445j.
- [52] D. Dannhauser *et al.*, "Biophysical investigation of living monocytes in flow by collaborative coherent imaging techniques," *Biomed. Opt. Express*, vol. 9, no. 11, p. 5194, 2018, doi: 10.1364/boe.9.005194.
- [53] N. Movilla, C. Borau, C. Valero, and J. García-Aznar, "Degradation of extracellular matrix regulates osteoblast migration: A microfluidic-based study," *Bone*, vol. 107, pp. 10–17, 2017, doi: 10.1016/j.bone.2017.10.025.
- [54] E. A. Sander and V. H. Barocas, "Comparison of 2D fiber network orientation measurement methods," *J. Biomed. Mater. Res.*, vol. 88A, no. 2, pp. 322–331, 2008.
- [55] E. Tzima *et al.*, "A mechanosensory complex that mediates the endothelial cell response to fluid shear stress," *Nature*, vol. 437, no. 7057, pp. 426–31, 2005.

This is the author's peer reviewed, accepted manuscript. However, the online version of record will be different from this version once it has been copyedited and typeset.
PLEASE CITE THIS ARTICLE AS DOI: 10.1063/5.0061997

- [56] D. Vestweber, "VE-cadherin: The major endothelial adhesion molecule controlling cellular junctions and blood vessel formation," *Arterioscler. Thromb. Vasc. Biol.*, vol. 28, no. 2, pp. 223–232, 2008, doi: 10.1161/ATVBAHA.107.158014.
- [57] E. S. Harris and W. J. Nelson, "VE-Cadherin: At the Front, Center, and Sides of Endothelial Cell Organization and Function," *Curr Opin Cell Biol*, vol. 2, no. 5, pp. 651–658, 2010, doi: 10.1016/j.ceb.2010.07.006.VE-Cadherin.
- [58] T. S. Frost, L. Jiang, R. M. Lynch, and Y. Zohar, "Permeability of epithelial/endothelial barriers in transwells and microfluidic bilayer devices," *Micromachines*, vol. 10, no. 8, 2019, doi: 10.3390/mi10080533.
- [59] A. Rabodzey, Y. Yao, F. Lusciuskas, S. Shaw, and C. F. Dewey, "Early response of endothelial cells to flow is mediated by VE-Cadherin," *Cell Commun. Adhes.*, vol. 14, no. 5, pp. 195–209, 2007, doi: 10.1080/15419060701755792.
- [60] S. Citi, "The mechanobiology of tight junctions," *Biophys. Rev.*, vol. 11, no. 5, pp. 783–793, 2019, doi: 10.1007/s12551-019-00582-7.
- [61] Y. Wallez and P. Huber, "Endothelial adherens and tight junctions in vascular homeostasis, inflammation and angiogenesis," *Biochim. Biophys. Acta - Biomembr.*, vol. 1778, no. 3, pp. 794–809, 2008, doi: 10.1016/j.bbamem.2007.09.003.
- [62] A. Boussommier-Calleja, Y. Atiyas, K. Haase, M. Headley, C. Lewis, and R. Kamm, "The effects of monocytes on tumor cell extravasation in a 3D vascularized microfluidic model," *Biomaterials.*, vol. 198, pp. 180–193, 2019, doi: 10.1016/j.biomaterials.2018.03.005.The.
- [63] O. Moreno-Arotzena, J. Meier, C. del Amo, and J. García-Aznar, "Characterization of Fibrin and Collagen Gels for Engineering Wound Healing Models," *Materials (Basel).*, vol. 8, no. 4, pp. 1636–1651, 2015, doi: 10.3390/ma8041636.
- [64] O. Moreno-Arotzena, C. Borau, N. Movilla, M. Vicente-Manzanares, and J. García-Aznar, "Fibroblast Migration in 3D is Controlled by Haptotaxis in a Non-muscle Myosin II-Dependent Manner," *Ann. Biomed. Eng.*, vol. 43, no. 12, pp. 3025–3039, 2015, doi: 10.1007/s10439-015-1343-2.
- [65] M. L. Kutys and C. S. Chen, "Forces and mechanotransduction in 3D vascular biology," *Curr. Opin. Cell Biol.*, vol. 42, pp. 73–79, 2016, doi: 10.1016/j.ceb.2016.04.011.
- [66] J. Huynh *et al.*, "Age-related intimal stiffening enhances endothelial permeability and leukocyte transmigration," *Sci. Transl. Med.*, vol. 3, no. 112, 2011, doi: 10.1126/scitranslmed.3002761.
- [67] C. Valero, H. Amaveda, M. Mora, and J. M. García-Aznar, "Combined experimental and computational characterization of crosslinked collagen-based hydrogels," *PLoS One*, vol. 13, no. 4, pp. 1–16, 2018, doi: 10.1371/journal.pone.0195820.
- [68] V. Olivares, M. Córdor, C. Del Amo, J. Asín, C. Borau, and J. M. García-Aznar, "Image-based characterization of 3d collagen networks and the effect of embedded cells," *Microsc. Microanal.*, vol. 25, no. 4, pp. 971–981, 2019, doi: 10.1017/S1431927619014570.
- [69] D. H. T. Nguyen *et al.*, "Biomimetic model to reconstitute angiogenic sprouting morphogenesis in vitro," *Proc. Natl. Acad. Sci. U. S. A.*, vol. 110, no. 17, pp. 6712–

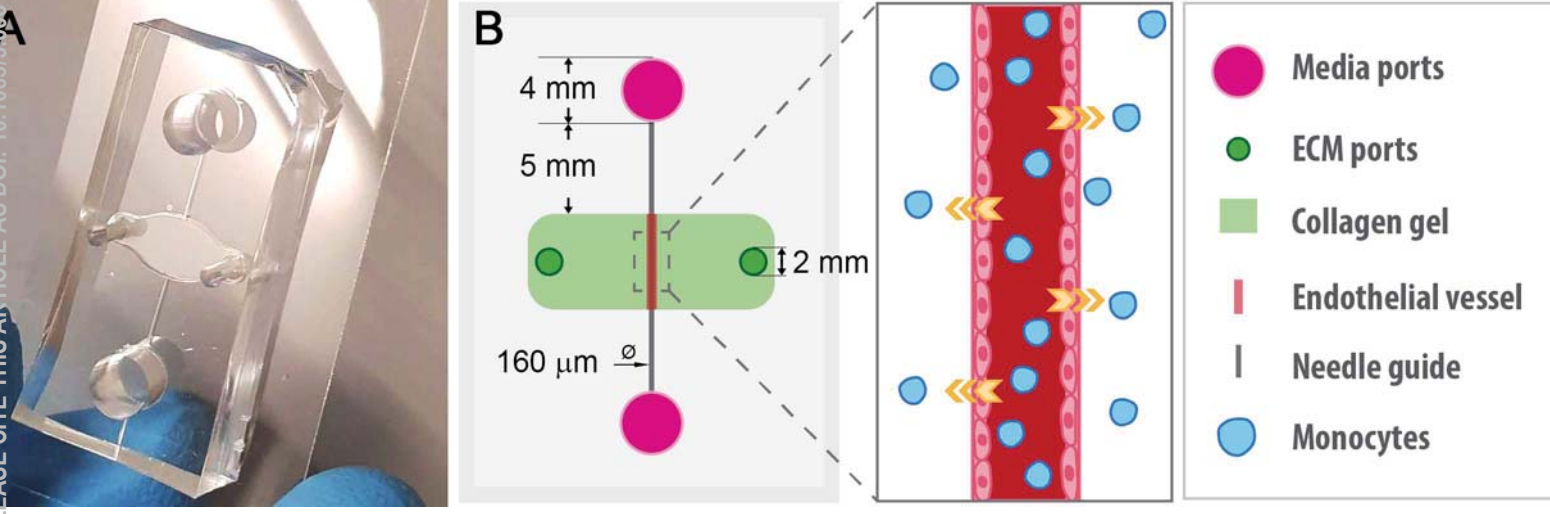
This is the author's peer reviewed, accepted manuscript. However, the online version of record will be different from this version once it has been copyedited and typeset.

PLEASE CITE THIS ARTICLE AS DOI: 10.1063/5.0061997

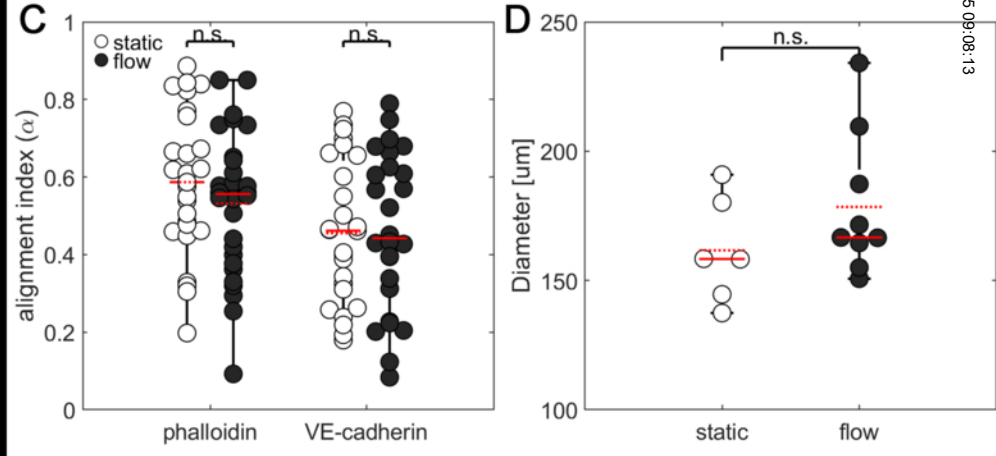
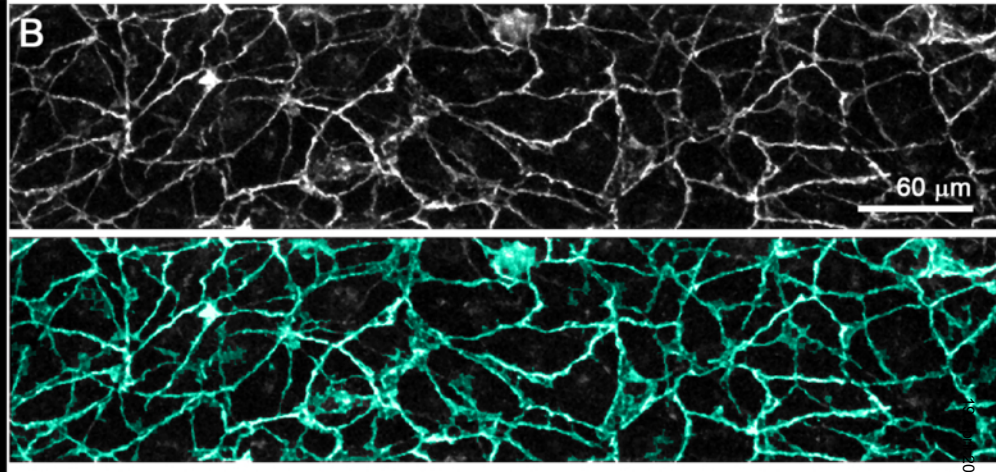
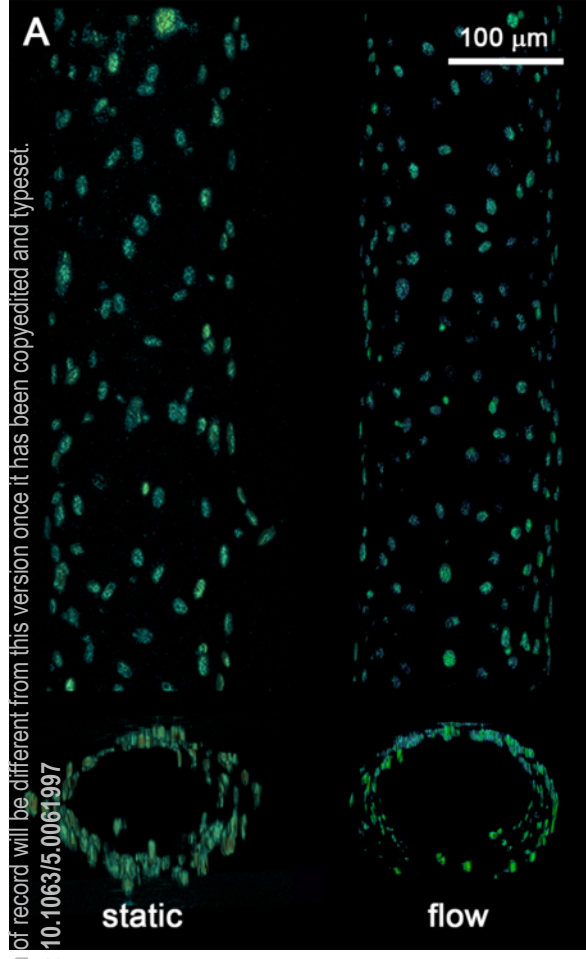
- 6717, 2013, doi: 10.1073/pnas.1221526110.
- [70] B. Trappmann, B. M. Baker, W. J. Polacheck, C. K. Choi, J. A. Burdick, and C. S. Chen, "Matrix degradability controls multicellularity of 3D cell migration," *Nat. Commun.*, vol. 8, no. 1, pp. 1–8, 2017, doi: 10.1038/s41467-017-00418-6.
- [71] M. M. Gong, K. M. Lugo-Cintron, B. R. White, S. C. Kerr, P. M. Harari, and D. J. Beebe, "Human organotypic lymphatic vessel model elucidates microenvironment-dependent signaling and barrier function," *Biomaterials*, vol. 214, no. 119225, 2019, doi: 10.1016/j.biomaterials.2019.119225.Human.
- [72] M. Virumbrales-Muñoz *et al.*, "Microfluidic lumen-based systems for advancing tubular organ modeling," *Chem. Soc. Rev.*, vol. 49, no. 17, pp. 6402–6442, 2020, doi: 10.1039/d0cs00705f.
- [73] J. Kreuger and M. Phillipson, "Targeting vascular and leukocyte communication in angiogenesis, inflammation and fibrosis," *Nat. Rev. Drug Discov.*, vol. 15, no. 2, pp. 125–142, 2016, doi: 10.1038/nrd.2015.2.
- [74] E. W. Baxter *et al.*, "Standardized protocols for differentiation of THP-1 cells to macrophages with distinct M(IFN γ +LPS), M(IL-4) and M(IL-10) phenotypes," *J. Immunol. Methods*, vol. 478, 2020, doi: 10.1016/j.jim.2019.112721.
- [75] A. Bah and I. Vergne, "Macrophage autophagy and bacterial infections," *Front. Immunol.*, vol. 8, no. NOV, pp. 1–9, 2017, doi: 10.3389/fimmu.2017.01483.
- [76] M. L. Kutys *et al.*, "Uncovering mutation-specific morphogenic phenotypes and paracrine-mediated vessel dysfunction in a biomimetic vascularized mammary duct platform," *Nat. Commun.*, vol. 11, no. 1, 2020, doi: 10.1038/s41467-020-17102-x.
- [77] S. Jalili-Firoozinezhad *et al.*, "A complex human gut microbiome cultured in an anaerobic intestine-on-a-chip," *Nat. Biomed. Eng.*, vol. 3, no. 7, pp. 520–531, 2019, doi: 10.1038/s41551-019-0397-0.

This is the author's peer reviewed, accepted manuscript. However, the online version of record will be different from this version once it has been copyedited and typeset.

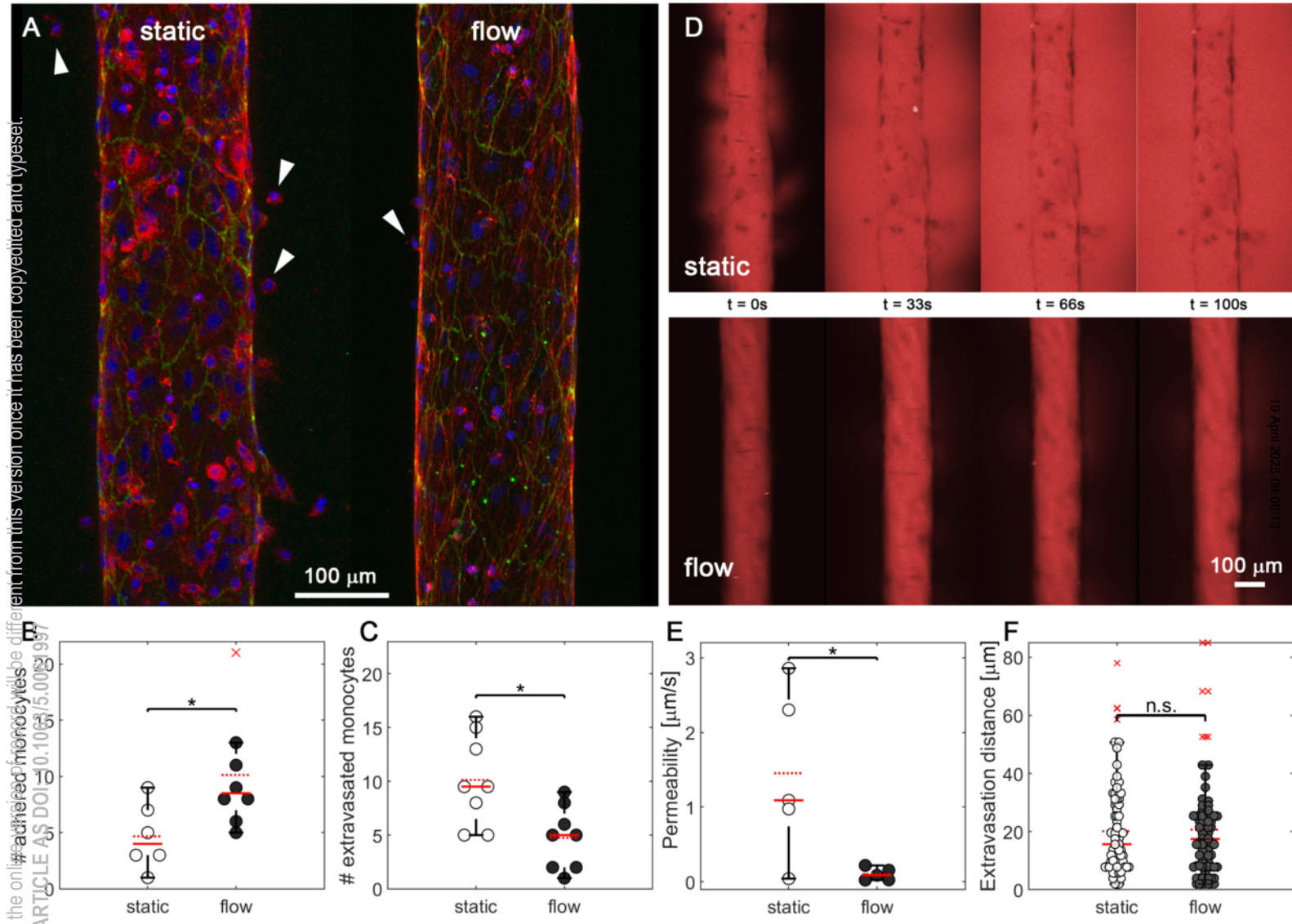
PLEASE CITE THIS ARTICLE AS DOI: 10.1063/1.50051997



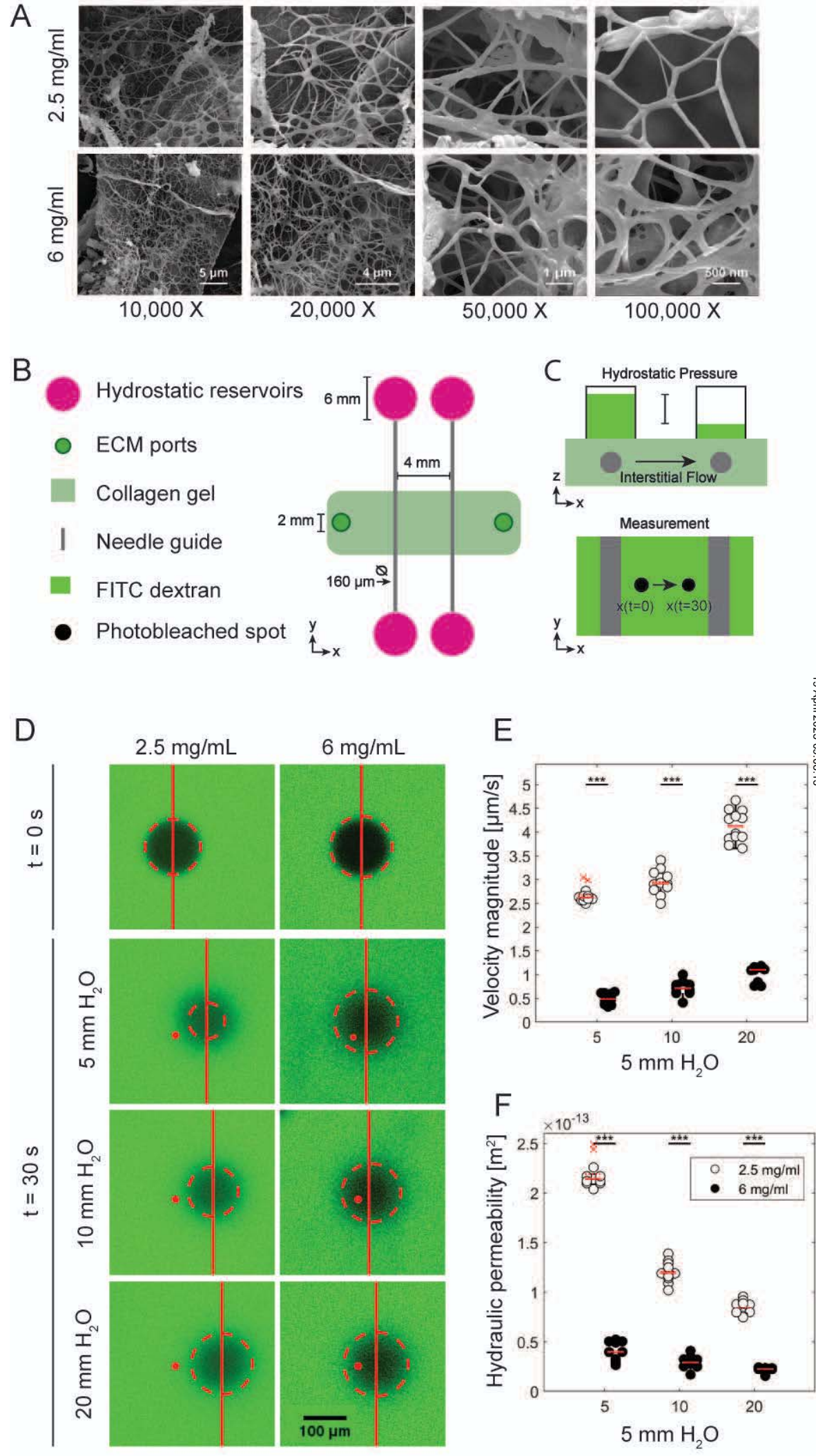
This is the author's peer reviewed, accepted manuscript. However, the online version of record will be different from this version once it has been copyedited and typeset.
PLEASE CITE THIS ARTICLE AS DOI: 10.1063/5.0061997



This is the author's peer reviewed, accepted manuscript. However, the online version of this article will be different from this version once it has been copyedited and typeset.
 PLEASE CITE THIS ARTICLE AS DOI: 10.1063/1.5003197



This is the author's peer reviewed, accepted manuscript. However, the online version of record will be different from this version once it has been copyedited and typeset.
 PLEASE CITE THIS ARTICLE AS DOI: 10.1063/1.50061997



This is the author's peer reviewed, accepted manuscript. However, the online version of record will be different from this version once it has been copyedited and typeset.
PLEASE CITE THIS ARTICLE AS DOI: 10.1063/5.0061997

